

# The role of momentum dependent dressing functions and vector meson dominance in hadronic light-by-light contributions to the muon $g-2$ .

Tobias Goecke,<sup>1</sup> Christian S. Fischer,<sup>1,2</sup> and Richard Williams<sup>3</sup>

<sup>1</sup>*Institut für Theoretische Physik, Universität Giessen, 35392 Giessen, Germany*

<sup>2</sup>*Gesellschaft für Schwerionenforschung mbH, Planckstr. 1 D-64291 Darmstadt, Germany.*

<sup>3</sup>*Institut für Physik, Karl-Franzens-Universität Graz, Universitätsplatz 5, 8010 Graz, Austria.*

We present a refined calculation of the quark-loop contribution to hadronic light-by-light scattering that focuses upon the impact of the transverse components of the quark-photon vertex. These structures are compared and contrasted with those found within the extended NJL-models. We discuss similarities and differences between the two approaches and further clarify the important role of momentum dependent dressing functions. As expected we find that the transverse structures of the quark-photon vertex lead to a suppression of the quark-loop contribution to the anomalous magnetic moment of the muon. However, we find evidence that this suppression is overestimated within models with simple approximations for the quark-photon interaction.

## I. INTRODUCTION

The anomalous magnetic moment of the muon  $a_\mu$  is an observable that furnishes a precision test of the electromagnetic (EM) interaction, the weak interaction and the strong interaction. The relative size of the different theoretical parts and comparison with the experimental results of the E821 experiment at Brookhaven [1, 2] are shown in table I. The dominant contribution of more than 99% is due to the EM interaction as described by quantum electrodynamics (QED), which has been evaluated up to order  $\alpha^5$  in the fine structure constant [3]. In addition, given the theoretical and experimental precision available, the weak interaction yields significant contributions [4]. An interesting feature of the observable  $a_\mu$  is its sensitivity to non-perturbative QCD corrections. The leading QCD contribution amounts to about 0.006% which is about two orders of magnitude larger than the total theory uncertainty. Together, the leading and sub-leading QCD contributions dominate the error of the total Standard Model prediction as can be seen in the table. This is because perturbation theory is not applicable and the methods used lead to a substantial error here. The two most relevant hadronic contributions are the hadronic vacuum polarisation (HVP) and the light-by-light (LBL) scattering contribution. The former

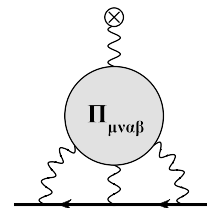


FIG. 1. The light-by-light scattering contribution to the muon  $g-2$ . The main ingredient is the hadronic photon four-point function  $\Pi_{\mu\nu\alpha\beta}$  to be discussed below.

is related to experimentally available  $e^+e^- \rightarrow \text{hadrons}$  data via dispersion relations (see [5]) and as such the error can be systematically reduced. This quantity is furthermore the subject of several recent lattice studies [6–8]. Furthermore, we have applied the method of Dyson-Schwinger equations (DSEs) to this quantity and were able to reproduce the dispersion analysis result on the ten percent level [9]. The result for HVP quoted in Table I is taken from Ref. [10]. Whilst presently the uncertainty is dominated by HVP, the LBL contributions (shown in Fig. 1) are potentially more problematic in the long run since it is extremely hard to determine these in a model-independent way. The LBL contributions have been investigated from the view point of low-energy effective models such as the Extended Nambu–Jona-Lasinio (ENJL) model [11], the Hidden Local Symmetry (HLS) model [12], vector meson dominance (VMD) approaches [13, 14], the non-local chiral quark model (NL $\chi$ QM) [15, 16], the chiral constituent quark model ( $\chi$ CQM) [17], in holographic models [18] and Dyson-Schwinger Equations [19, 20]. The lattice calculations of LBL are still at an exploratory stage [21]. The LBL-contribution quoted in Table I is taken from Ref. [22]. There different groups, pursuing the strategy of hadronic models, agreed on this number.

A future experiment, to be conducted at Fermilab, will measure the anomalous magnetic moment of the muon  $a_\mu$  to a precision of 0.14 ppm [23]. It is thus mandatory to

Contribution	$a_\mu \times 10^{11}$	$\frac{a_\mu^i}{a_\mu^{SM}}$	$\left(\frac{\delta a_\mu^i}{\delta a_\mu^{SM}}\right)^2$
QED	116 584 718.1 ( 0.2 )	99.99390%	00.00098%
weak	153.2 ( 1.8 )	00.00013%	00.07910%
QCD LOHVP	6 949.1 (58.2)	00.00596%	82.69628%
QCD HOHVP	−98.4 ( 1.0 )	00.00008%	00.02441%
QCD LBL	105 ( 26 )	00.00009%	16.50391%
Standard Model	116 591 827.0 (64 )	100%	100%
Experiment	116 592 089 ( 63 )		
Exp-Theo	262 ( 89 )		

TABLE I. Standard Model contributions to the muon  $g-2$ .

work towards getting the LBL contribution under sufficient control. For this undertaking we require mature non-perturbative methods that are well-rooted in QCD, such as DSE's and lattice QCD. We believe that a promising way for the future is to combine these methods in a complementary fashion.

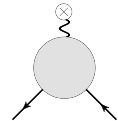
In previous works we have determined important parts of the hadronic LBL contributions such as pseudoscalar meson exchange and non-transverse contributions to the quark-loop part of LBL [19, 20]. What has been left out so far are the transverse structures of the quark-photon coupling due to numerical complexity. From vector-meson dominance models, however, these contributions are believed to be sizable and negative and therefore lead to a substantial overall reduction of the LBL contribution to the muons anomalous magnetic moment. A complete approach towards LBL therefore has to include these contributions explicitly. In this work we provide a further step into this direction. The main focus of this article is, however, on the comparison between our approach and models like the ENJL or chiral quark model. We will argue that such models provide simple tools to give important qualitative insights into the significance of different contributions to LBL. However, in order to provide more precise quantitative results, more elaborate approaches that take into account the full momentum dependence of dressing functions are mandatory.

This paper is organized as follows. First we briefly introduce the quantity under question and give the Dyson-Schwinger Equations (DSE) and the particular truncation used in this work, together with some notation, in section II. In section III we introduce the hadronic four-point function that lies at the heart of the LBL contribution and define it in terms of Green's functions. The main body of this work, the quark loop contribution to LBL, is discussed at length in section IV. Here we make comparison between the DSE and the ENJL approach in order to highlight similarities and differences. This is followed by a detailed discussion of our numerical results in section V, where the main focus is on the influence of momentum dependent dressing functions and the different structures in the self-consistent quark photon vertex that are a vital part of our calculation. Details concerning the quark-photon vertex and the derivation of the hadronic four-point tensor in the present truncation are given in the appendix.

## II. BASICS

To obtain the LBL contribution to the muon anomalous magnetic moment  $a_\mu^{\text{LBL}}$  one must consider its contribution to the muon-photon vertex shown in Fig. 1. On

the muon mass-shell this vertex can be decomposed as



$$= \bar{u}(p') \left[ F_1(q^2) \gamma_\alpha + i F_2(q^2) \frac{\sigma_{\alpha\beta} q^\beta}{2m_\mu} \right] u(p), \quad (1)$$

where  $p$  and  $p'$  are the muon momenta,  $q$  is the photon momentum and  $\sigma_{\alpha\beta} = \frac{i}{2}[\gamma_\alpha, \gamma_\beta]$ . The anomalous magnetic moment is defined as

$$a_\mu = \frac{g - 2}{2} = F_2(0), \quad (2)$$

which is obtained from Eq. (1) in the limit of vanishing photon momentum,  $q^2$ . Here we will use the technique advocated in Ref. [24] which simplifies the numerics by ensuring that all integrals are explicitly finite, see Ref. [20] for details.

In the following we introduce the Dyson-Schwinger equations for the quark propagator and the quark-photon vertex, together with the truncation scheme used in our calculations. The dressed quark propagator is given by

$$S^{-1}(p) = Z_f^{-1}(p^2) (-i\not{p} + M(p^2)), \quad (3)$$

where  $Z_f(p^2)$  is the quark wave-function renormalisation and  $M(p^2)$  is the quark mass function. These scalar functions are obtained as solutions to the quark DSE,

$$S^{-1}(p) = Z_2 S_0^{-1} + g^2 Z_{1f} \frac{4}{3} \int \overline{d}k \gamma^\mu S(k) \Gamma^\nu(k, p) D_{\mu\nu}(q), \quad (4)$$

where  $\overline{d}k = d^4k/(2\pi)^4$  and  $q = k - p$  is the gluon's momentum. The bare inverse quark propagator is  $S_0^{-1}(p) = -i\not{p} + m_0$ . This bare mass is related to the renormalized one by  $Z_2 m_0 = Z_2 Z_m m_q$ , with  $Z_2$  and  $Z_m$  the wave-function and quark-mass renormalisation constants. The renormalisation constant for the quark-gluon vertex is  $Z_{1f}$ . To solve Eq. (4) we need the gluon propagator  $D_{\mu\nu}(q)$  and the quark-gluon vertex  $\Gamma^\nu(k, p)$ .

The quark-gluon interaction that appears in the DSE for the quark reads:

$$Z_{1f} \frac{g^2}{4\pi} D_{\mu\nu}(q) \Gamma_\nu(k, p). \quad (5)$$

In Landau gauge,  $D_{\mu\nu} = T_{\mu\nu}(q)Z(q^2)/q^2$  where the transverse projector is  $T_{\mu\nu}(q) = \delta_{\mu\nu} - q_\mu q_\nu/q^2$ . The quark-gluon vertex  $\Gamma_\nu(k, p)$  can be decomposed into twelve Dirac covariants. However, we will employ the rainbow-ladder (RL) truncation, which requires that we replace the complicated structure of the quark-gluon vertex with just its  $\gamma_\mu$  component. Hence Eq. (5) becomes

$$Z_{1f} \frac{g^2}{4\pi} T_{\mu\nu}(q) \frac{Z(q^2)}{q^2} \Lambda(q^2) \gamma_\nu, \quad (6)$$

where  $\Lambda(q^2)$  is the non-perturbative dressing of the  $\gamma_\nu$  part of the quark-gluon vertex, restricted to depend only on the exchanged gluon momentum. Combining all scalar

dressings into one effective running coupling,  $\alpha_{\text{eff}}(q^2)$  we have

$$Z_{1f} \frac{g^2}{4\pi} D_{\mu\nu}(q) \Gamma_\nu(k, p) = Z_2^2 T_{\mu\nu}(q) \frac{\alpha_{\text{eff}}(q^2)}{q^2} \gamma_\nu, \quad (7)$$

where  $\alpha_{\text{eff}}$  is a renormalization group invariant. The factor  $Z_2^2$  ensures multiplicative renormalizability.

In contemporary Dyson-Schwinger studies one employs the Bethe-Salpeter equations to study bound states of two particles, with the interaction described by a two-body kernel. To provide a realistic description of pseudoscalar mesons one requires that the dynamical breaking of chiral symmetry is encoded into the truncation. The symmetry-preserving two-body kernel corresponding to this yields the ‘ladder’ part of RL. For simplicity we quote this in terms of  $\alpha_{\text{eff}}$ ,

$$K_{rs,tu}(q) = 4\pi Z_2^2 \frac{\alpha_{\text{eff}}(q^2)}{q^2} T_{\mu\nu}(q) [\gamma^\mu]_{rt} [\gamma^\nu]_{us}. \quad (8)$$

Note that it is possible to employ a beyond-RL truncation here, see Refs. [25–29]. In practice such an extension complicates the numerics considerably and is therefore not yet viable in the context of  $g = 2$ .

We will employ an effective interaction called the Maris-Tandy (MT) model which has much phenomenological success for pseudoscalar and vector meson masses, decay constants and form factors [30–34]. Success in the meson sector has led to its widespread use in the calculation of baryon properties [35–38]. This effective running coupling is given by

$$\alpha_{\text{eff}}(q^2) = \pi \frac{D}{\omega^2} x^2 e^{-x} + \frac{2\pi\gamma_m(1 - e^{-y})}{\log[e^2 - 1 + (1 + z)^2]}, \quad (9)$$

$$x = q^2/\omega^2, \quad y = q^2/\Lambda_t^2, \quad z = q^2/\Lambda_{QCD}^2,$$

and features a Gaussian distribution in the infrared that provides dynamical chiral symmetry breaking. It is characterized by an energy scale  $(\omega D)^{1/3} = 0.72$  GeV, fixed to give the pion decay constant, and we choose  $\omega = 0.4$  GeV. The second part reproduces the one-loop running coupling at large perturbative momenta. It includes the anomalous dimension  $\gamma_m = 12/(11N_C - 2N_f)$  of the quark propagator, and we use  $\gamma_m = 12/25$ ,  $\Lambda_{QCD} = 0.234$  GeV and  $\Lambda_t = 1$  GeV. Note that we also employ a Pauli-Villars like regulator with a mass scale of 316 GeV. We focus here on the two lightest quarks whose mass at  $\mu = 19$  GeV is 3.7 MeV.

The equation for the quark-photon vertex can be written in the form of an inhomogeneous Bethe-Salpeter equation in rainbow-ladder truncation, dependent upon the same two-body ladder kernel Eq. (8)

$$[\Gamma_\mu(P, k)]_{rs} = Z_1 \gamma_\mu \quad (10)$$

$$- Z_2^2 \frac{4}{3} \int \bar{d}q [S(q_+) \Gamma_\mu(P, q) S(q_-)]_{ut} K_{tu,rs}(k - q),$$

where  $\bar{d}q = d^4q/(2\pi)^4$ ,  $P$  is the outgoing photon momentum,  $q_\pm = q \pm P/2$ , and  $Z_1$  (by the Ward identity  $Z_1 = Z_2$ ) is the renormalization constant of the

quark-photon vertex. The use of rainbow-ladder here ensures that the important vector and axial-vector Ward-Takahashi identities (WTIs) hold [39, 40].

For our purposes it is reassuring to have a description that is able to reproduce a number of observables whilst at the same time being sufficiently simple that we can define unambiguously the hadronic four-point function. Furthermore, this approach describes at the same time both the perturbative and non-perturbative regime. This unification of IR and UV scales is very important for the problem of LBL and is not shared by effective low-energy descriptions of the strong interaction. The importance of this feature will be elaborated in section IV.

### III. CONTENT OF THE HADRONIC FOUR-POINT FUNCTION.

Now we turn to the structure of the hadronic photon four-point function  $\Pi_{\mu\nu\alpha\beta}$ , central to the computation of the hadronic LBL contributions. Using the rainbow-ladder truncation as introduced above, this object can be written exactly in the form (see Appendix B)

$$\text{Diagram} = 6 \text{Diagram}_1 + 12 \text{Diagram}_2, \quad (11)$$

where the factors 6 and 12 indicate the number of permutations of the diagrams that one must consider. We see that there are two classes of diagrams:

- The second class of diagram contains the T-matrix that describes all kinds of quark-antiquark interactions including the dynamical propagation of mesons. In our earlier work, the T-matrix was approximated by pseudoscalar meson exchange [19, 20] in reasonable agreement with low energy effective models [11, 13–15, 17, 22, 41–46].
- The first diagram, which we refer to as the quark-loop topology, will constitute the main focus of this work. This object is composed entirely of fully dressed quark propagators and quark-photon vertices. In our previous publications [19, 20] we were not in a position to employ here the full quark-photon vertex as described by Eq. (10) due to the numerical complexity. Instead, we were limited to the Ball-Chiu construction [47] that fixes the first four components of Eq. (A1) exactly in terms of the quark dressing functions, see Eq. (A3).

In this work we will investigate the leading transverse structure that, amongst other things, dynamically yield the picture of vector meson dominance (VMD) [32]. This is the case since these structures couple to the vector meson channel and hence one finds time-like poles corresponding to bound states. The leading component will be extracted and compared with its ENJL equivalent.

Note that we will limit the considerations to the case of two degenerate flavors for simplicity. The contributions of strange and charm quarks are only included for our best estimate of the LBL contribution in section V D.

Note that there are contributions in the four-point function that are not accounted for in the representation of Eq. (11). These include unquenching effects due to internal quark lines that can be connected to the dynamical back-coupling of hadronic degrees of freedom [48]. In effective descriptions such contributions show up as pion-loops that organise themselves into a counting scheme within chiral perturbation theory. These contributions are typically considered to be sub-leading. A recent investigation, however, finds that next-to-leading order contributions might be more important than expected due to the somewhat accidental smallness of the leading terms [49].

#### IV. QUARK LOOP: COMPARING DSE TO ENJL

In principle we have all of the ingredients at our disposal, see Eqs. (1,2) to calculate the quark-loop contribution to LBL shown in Fig. 2. We note that this involves a three-loop integration over fully dressed quark propagators and quark-photon vertices which poses a considerable numerical challenge. Thus, to err on the side of caution we present a step-wise investigation of going beyond the tree-level approximation reported in [19].

Additionally, it is useful to put our calculation in perspective so that a greater understanding of our approach can be conveyed. To this end, we will present a comparison between the DSE approach and the, in many ways similar, ENJL model [50]. There are of course subtle differences between the two, and we will here point out, contrast, and discuss the consequences of each. This we further cement by testing ENJL-inspired vertices within our approach to explicate their kinematical differences.

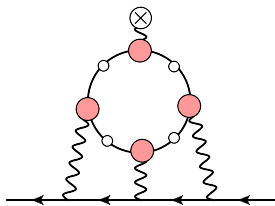


FIG. 2. The quark loop contribution to the muon  $g - 2$ . The quarks and vertices are dressed according to Eqs. (4,10).

#### A. The ENJL perspective

The inverse quark propagator in the ENJL model is just

$$S_{\text{ENJL}}^{-1}(p) = -i\not{p} + M, \quad (12)$$

with  $p$  a Euclidean momentum and  $M$  the constituent quark mass. Note that the wave function renormalisation is just unity and the mass function is independent of momentum.

The quark-photon vertex is given here by a bubble sum

$$\text{wavy line} \left( + \text{wavy line} \begin{array}{c} \circ \\ \circ \\ \circ \end{array} \right), \quad (13)$$

see Refs. [11, 51] for details. Owing to the simple structure of the effective four-quark vertices, the contributions can be resummed as a simple geometric series of one-loop amplitudes  $\sum_n \text{Bubble}^n = 1/(1 - \text{Bubble})$ . As a result, the quark-photon vertex depends only on the photon momentum  $Q^2$  and not on the relative momentum of the quarks<sup>1</sup>.

Thus we have

$$\Gamma_{\mu}^{\text{ENJL}}(Q) = \gamma_{\mu} - g_{\text{ENJL}} \Pi_{\mu\nu}(Q) \gamma_{\nu}, \quad (14)$$

where  $g_{\text{ENJL}}$  is derived from standard NJL couplings.

The bubble sum  $\Pi_{\mu\nu}(Q)$  has the transverse structure

$$\Pi_{\mu\nu}(Q^2) = (Q^2 \delta_{\mu\nu} - Q_{\mu} Q_{\nu}) \Pi^{\text{T}}(Q^2), \quad (15)$$

since a potential longitudinal piece  $\Pi^{\text{L}}(Q^2)$  vanishes for identical quark masses [51].

According to Ref. [51] the transverse part in the VMD limit has the form

$$\Pi^{\text{T}}(Q^2) = \frac{2f_V^2 M_V^2}{M_V + Q^2}, \quad (16)$$

where the momentum dependence of the mass function  $M_V$  and decay constant  $f_V$  are neglected, which is reported to be a rather good approximation to the momentum dependent case. In the limit we consider here,  $2f_V^2 M_V^2 = 1/g_{\text{ENJL}}$  and so

$$\Gamma_{\mu}^{\text{ENJL}} = \gamma_{\mu} - \gamma_{\mu}^{\text{T}} \frac{Q^2}{Q^2 + M_V^2}, \quad (17)$$

where  $\gamma_{\mu}^{\text{T}} = \gamma_{\nu} T_{\mu\nu}(Q)$  and  $M_V$  is identified with the mass of the  $\rho$ -meson. Together with the quark propagator Eq. (12) the vertex satisfies the vector Ward-Takahashi identity (WTI), Eq. (A2). Note that the vertex in Eq. (17) can be written as  $\sim \gamma_{\mu} M_V^2 / (Q^2 + M_V^2)$  if the quark loop is transverse. This explicates why a suppression is found for VMD inspired transverse dressings compared to a bare vertex  $\gamma_{\mu}$ .

<sup>1</sup> Note that a similar simplification happens for the four-quark T-matrix, which essentially reduces to a bubble sum sandwiched between two pairs of quark legs. The resulting mesons are point-like objects.

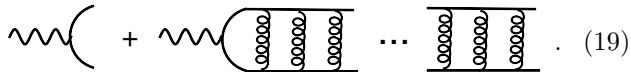
## B. The DSE perspective

In the DSE approach, the inverse quark propagator has the following covariant decomposition

$$S_{\text{DSE}}^{-1}(p) = Z_f^{-1}(p^2) (-i\not{p} + M(p^2)), \quad (18)$$

where in contrast to Eq. (12) we have a momentum dependent wave function  $Z_f(p^2)$  and mass function  $M(p^2)$ .

In the rainbow-ladder truncation employed here, the quark-photon vertex is a dressed ladder-resummation of effective gluons



$$\text{---} \left( + \text{---} \left( \text{---} \right) \dots \left( \text{---} \right) \right). \quad (19)$$

If we replace the gluon exchange by a momentum independent contact interaction we arrive at a picture similar to the ENJL model above. Keeping the exchange as is, the calculation is somewhat more involved as we can no longer have a simple geometric series.

The full quark-photon vertex is given by

$$\Gamma_\mu(Q, k) = \sum_{i=1}^4 \lambda^{(i)} L_\mu^{(i)}(Q, k) + \sum_{i=1}^8 \tau^{(i)} T_\mu^{(i)}(Q, k), \quad (20)$$

with  $\lambda^{(i)} = \lambda^{(i)}(Q^2, k^2, Q \cdot k)$  and  $\tau^{(i)} = \tau^{(i)}(Q^2, k^2, Q \cdot k)$  the longitudinal and transverse scalar coefficients respectively that correspond to the basis elements given in Eq. (A1). Additionally  $\Gamma_\mu^{\text{BC}} = \sum_{i=1}^4 \lambda^{(i)} L_\mu^{(i)}(Q, k)$  defines the Ball-Chiu vertex with the coefficients fixed by the vector WTI [47]. Our main interest here lies in the eight transverse components  $T_\mu^{(i)}(Q, k)$  which couple to vector bound-states. For the sake of comparison with the ENJL model, we will take only the leading transverse component  $T_\mu^{(1)}(Q, k) = \gamma_\mu^T$  under consideration in this work.

While we are mainly working with the full numerical result for the quark-photon vertex it is sometimes useful to also have a simple analytical form at hand, which captures the main features of the numerical solution. An approximate form for the leading component of the transverse part has been given in Ref. [32] which depends on both the relative and total momenta of the vertex

$$\Gamma_\mu(Q, k) \simeq \Gamma_\mu^{\text{BC}} - \gamma_\mu^T \frac{\omega^4 N_V}{\omega^4 + k^4} \frac{f_V}{M_V} \frac{Q^2}{Q^2 + M_V^2} e^{-\alpha(Q^2 + M_V^2)}. \quad (21)$$

This form has been fitted to the full numerical solution for the quark-photon vertex obtained from its BSE. Here,  $\omega$  and  $\alpha$  describe the suppression of the amplitude for large relative and total momentum respectively. We find reasonable agreement with the numerical solution with  $\omega = 0.66 \text{ GeV}$ ,  $\alpha = 0.15$  and  $N_V f_V / M_V = 0.152$ , see Fig. 5. Additionally,  $N_V$  is a normalization factor. We consider this formula to be the VMD limit of the DSE quark-photon vertex. In addition to this BSE inspired

fit, we will also employ the  $T_\mu^{(1)}$  component of the vertex as extracted from the full calculation of the quark-photon vertex BSE.

## C. Differences between DSE and ENJL

One of the key differences between the ENJL and DSE approaches is that in the former we have a contact interaction, whilst the latter features an interaction that features momentum exchange. This has far-reaching consequences as we discuss below.

Firstly we look at the differences in the quark propagator, see Fig. 3. In the ENJL model we have  $Z_f(p^2) = 1$  and  $M(p^2) = M_{\text{const}}$  as opposed to the fully momentum dependent functions from the DSE. For the quark mass function, we see that in the DSE it saturates in the IR at about  $M(0) \approx 450 \text{ MeV}$  and continuously connects to its perturbative running at large momenta. The ENJL model, in contrast features a constituent-like quark mass of  $\sim 300 \text{ MeV}$  at all scales up until the model cut-off

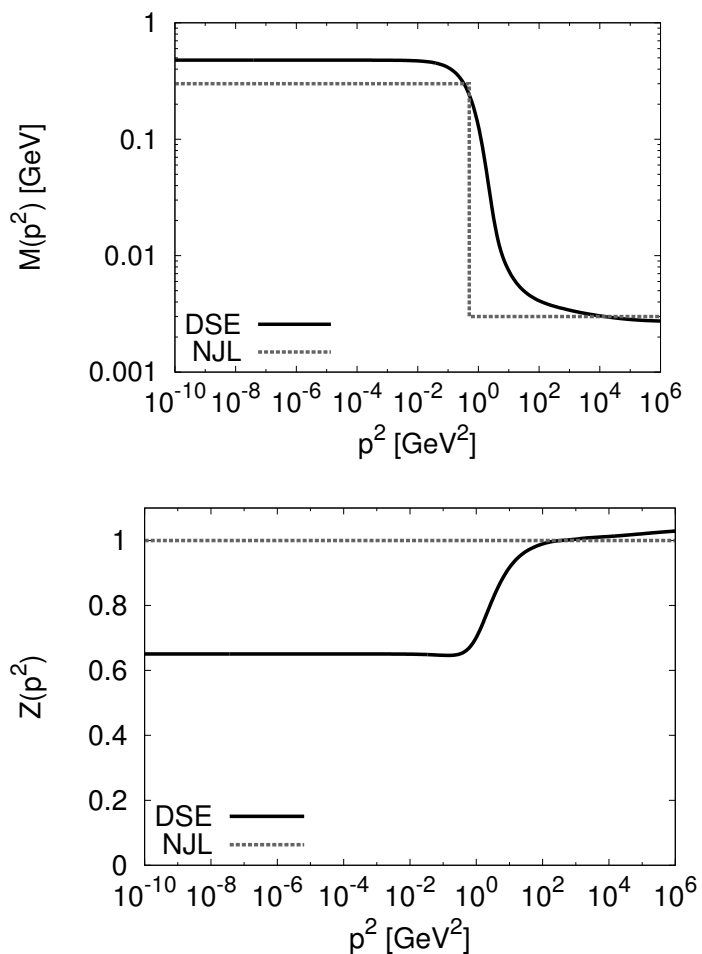


FIG. 3. Comparison of the mass function  $M$  and the wave function  $Z_f$  for DSE and ENJL quarks.

$\sim 1$  GeV. For the quark wave function renormalisation, we see that for a large momentum range  $Z_f(p^2) < 1$  which constitutes a suppression of the quark propagator with respect to the constant  $Z$  of the ENJL model. This can have several consequences for the quark-loop contribution to  $g - 2$ , Fig. 2, where there are four quark propagators. With  $Z_f(p^2) < 1$  in the DSE approach, we may expect a suppression of the contribution by a factor  $Z_f(s)^4$  for some representative, ‘average’ momentum scale  $s$ . On the other hand, the momentum dependent quark-mass function allows for quark masses smaller than  $M(p^2 = 0)$  to be probed. Naively, this leads to an enhancement of the contribution. This may be equivalent to using a momentum-independent quark mass  $M(s)$  where  $s$  is some representative momentum scale. This ‘effective’ mass may be surprisingly small and, indeed, such small quark masses have been observed to be necessary in several models [15, 17, 52]. We come back to this point below.

If we now compare the ENJL vertex, Eq. (17) and its DSE equivalent, Eq. (21) we see that there is a similar structure. That is, there is a part dictated by the WTI (gauge part) and a part that represents the VMD physics of the transverse vertex. Whilst in the case of the DSE we have functions that depend on both the photon and relative quark momenta, in the case of the ENJL model we have trivial momentum dependence for the gauge-part, and reduced momentum dependence for the transverse part.

First, let us discuss the gauge part of the quark-photon vertices. The leading coefficient of  $\gamma_\mu$  has the form

$$\lambda^{(1)}(Q^2, k^2, k \cdot Q) = \frac{1}{2} \left( \frac{1}{Z_f(k_+^2)} + \frac{1}{Z_f(k_-^2)} \right), \quad (22)$$

where  $k_\pm = k \pm Q/2$ . Based on the difference in behavior of the quark propagators, we see for the ENJL model that  $\lambda_1 = 1$ , whilst for the DSE  $\lambda_1 > 1$ . Thus, for the DSE we expect the gauge part of the vertex to yield an enhancement of the quark-loop  $\sim 1/Z_f(s)^4$  as to the bare vertex approximation. A comparison of these components of the vertex is shown in Fig. 4.

Now we take a look at the dominant transverse component of the quark-photon vertex. In Fig. 5 we show the dressing function as calculated self-consistently from the DSE for the quark-photon vertex, together with the fit function of Eq. (21) and the equivalent part of the ENJL vertex, Eq. (17). We see that the fit to the DSE, as a function of the total momentum  $Q$ , behaves very similarly as the full numerical solution in the dominant region around the scale  $M_V = 0.77$  GeV. Small deviations occur at large momenta due to the exponential fall-off of the fit function. The dressing function of the ENJL model has a similar behavior except at large momenta where no fall-off is seen and instead it tends to a constant. However, due to the weighting of the integrand in the calculation of  $a_\mu$  it transpires that such deviations at large  $Q^2$  are not relevant.

However, differences between the DSE and ENJL approach become readily apparent when one considers the impact of the relative momentum on the kinematics. In the DSE approach the transverse VMD-piece is suppressed for momenta  $k^2 \gtrsim \omega^2 \approx \Lambda_{\text{QCD}}^2$ , an effect which is not present in the ENJL approach due to its contact interaction. As a consequence, we expect smaller negative contributions to LBL in the DSE approach as compared to ENJL. The degree of overestimation of negative contributions in ENJL depends upon the kinematical weighting of the integrand, and can be estimated in our approach by systematically removing the dependence on the relative momentum in our quark-vertex dressing function. This will be detailed in the next section.

## V. RESULTS

Here we present a more quantitative analysis of the difference between the ENJL and DSE approaches, with respect to various approximations that can be made in

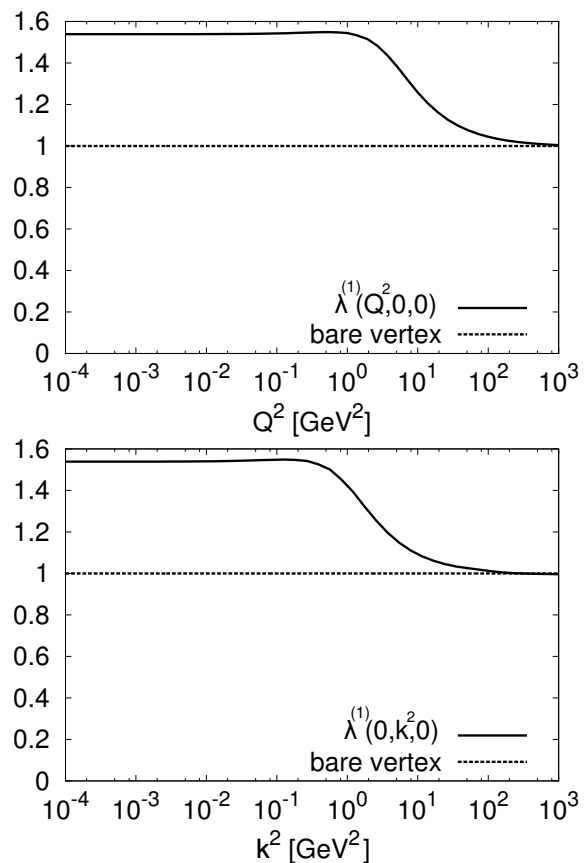


FIG. 4. The leading  $\lambda^{(1)}$  component of the quark-photon vertex constrained by the Ward-Takahashi identity of Eq. (A2) and given in Eq. (22). We show two slices as a function of the total and relative momenta  $Q^2$  (with  $k = 0$ ) and  $k^2$  (with  $Q = 0$ ), respectively. Note that the constant dressing corresponds to the ENJL model.

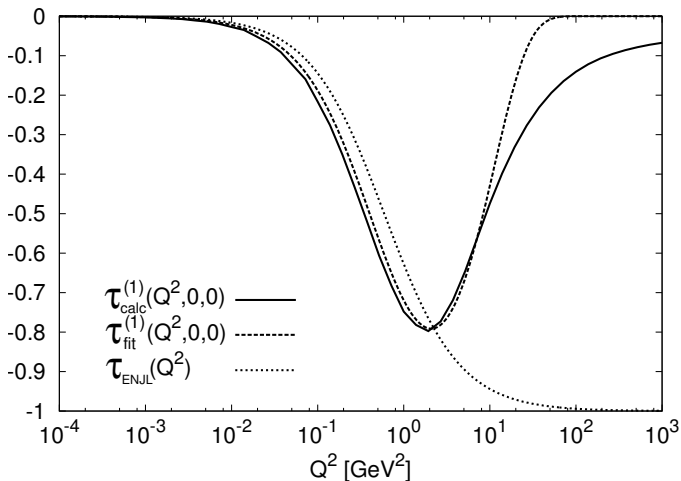


FIG. 5. The dependence of the dominant transverse dressing  $\tau^{(1)}$  on the photon momentum  $Q^2$  is shown for the explicit solution of the quark-photon vertex BSE, Eq. (10), the fit to this given in Eq. (21), and the transverse part of the ENJL vertex, Eq. (17).

the calculation of the quark loop. In order to compare the two approaches we need a means to find the most important and therefore representative momentum scales. This we achieve by averaging over the dressing functions, as weighted by the importance sampling of the VEGAS Monte-Carlo [53] we use to evaluate the quark-loop contribution to LBL.

For the calculation in the DSE-framework we use an IR-cutoff of  $10^{-3}$  GeV and an UV-cutoff of  $10^3$  GeV for all three loop variables. No additional splitting into a perturbative and a nonperturbative region is necessary, since these regions are continuously connected, see the discussion around Fig. 3. In contrast, this is different for the ENJL model where the calculation is split into a low and a high-energy part [11]. In the former, constituent quarks Eq. (12) with  $M = 0.3$  GeV are used together with the vertex construction Eq. (17). This low-energy part is cut off by requiring the photon momenta to be  $q \leq \mu$ , where  $\mu$  is varied in the range between 0.7 GeV and 4 GeV. The high-energy contribution is approximated by a bare quark-loop (bare propagators and bare vertices) where the mass of the quarks is given by the same scale  $\mu$  which is supposed to act as an effective IR-cutoff. It was found in [11] that the result is rather stable against a variation of  $\mu$  in the considered range. The final result is quoted as

$$a_\mu^{\text{LBL,ql,ENJL}} = 21(3) \times 10^{-11}. \quad (23)$$

Note that if  $\mu = 4$  GeV is taken, almost the complete contribution comes from the low-energy part. While this value is usually considered to be inappropriately high for an NJL type model, we find this viewpoint useful since it facilitates the comparison to the DSE case, where there

Quark dressing	$\langle Z_f \rangle$	$\sqrt{\langle M^2 \rangle}$ [GeV]	$a_\mu [10^{-11}]$
$Z_f$ and $M$ dynamical	0.83	0.14	47
$Z_f = Z_2^{-1}$ , $M$ dynamical	–	0.18	102
$Z_f = Z_2^{-1}$ , $M = 0.477$	–	–	22
$Z_f = Z_2^{-1}$ , $M = 0.300$	–	–	51
$Z_f = Z_2^{-1}$ , $M = 0.200$	–	–	104

TABLE II. The quark-loop contribution to hadronic LBL together with effective average values for the  $Z_f$  and  $M$  functions determined with a bare quark-photon vertex  $Z_2\gamma_\mu$ . We compare results for dynamical quark dressing functions to those with static ENJL-like equivalents. The quark wavefunction renormalisation point constant  $Z_2 \approx 0.97$  for the cutoff and renormalisation point used.

is no separation in high and low-energy parts. We will later see that the contribution Eq. (23) can be roughly reproduced even with the much higher cutoff we use in our calculations<sup>2</sup>. The results presented in this work are obtained within Landau gauge for QED ( $\xi = 0$  in the photon propagator apparent in fig. 2), in contrast to our earlier work [19, 20] where we used Feynman gauge for QED ( $\xi = 1$ ). It turns out that all the results presented here are affected only mildly by this choice, as can be seen in Table VI.

#### A. Impact of a dynamical $Z_f$ and $M$

To gauge the impact of momentum dependent quark dressing functions, we compare several calculations in the bare-vertex approximation, see Table II. Note that we attach a renormalisation constant to the bare vertex e.g.  $Z_2\gamma_\mu$  to ensure multiplicative renormalisability. For a momentum independent quark wave-function we also supplement the quark by a factor  $Z_2^{-1}$  for the same reason. These extra factors cancel in all but the first line of Table II. The corresponding case of bare vertex with fully dressed quark thus differs from our earlier results [19, 20] by a factor of  $Z_2^4 \approx 0.89$  in addition to the different QED gauge and the smaller number of quark flavours.

Let us first compare the first two lines of Table II. Replacing the dynamical quark wave function by  $Z_f = Z_2^{-1}$  we note an enhancement of the contribution to  $a_\mu$  roughly by a factor of 2. This is in good agreement with the expectation discussed above: since there are four quark propagators in the quark loop, the full calculation contains an extra factor of the order  $\langle Z_f \rangle^4$  with  $\langle Z_f \rangle$  the average value of the wave-function that is probed. Indeed, one finds  $\langle Z_f \rangle^4 \simeq (0.83)^4 \sim 0.5$ .

<sup>2</sup> Note furthermore that Eq. (23) includes strange quarks which we neglect in this work. These give, however, a few percent correction [11] such that this detail is not important for the more general analysis we present here.

Quark Dressing	$\langle Z_f \rangle$	$a_\mu [10^{-11}]$
$Z_f$ and $M$ dynamical	0.76	100

TABLE III. The quark-loop contribution to hadronic LBL with the 1BC dressing and the average of the  $Z_f$  function. These are to be compared with the bare-vertex results in the previous table.

To explore the impact of the momentum dependent quark mass function, we keep  $Z_f = Z_2^{-1}$  fixed and compare several constant values of  $M$  to the dynamical case. For  $M = 0.477$  GeV, the infrared plateau of the dynamical mass function, we obtain less than 1/5th of the dynamical result (with  $Z_f = Z_2^{-1}$ ). A quark mass of  $M = 0.3$  GeV gives a result commensurate with the calculation of Ref. [54] which yields  $a_\mu^{L_{BL}, ql, N_f=2} = 49.1(3.4) \times 10^{-11}$  for the contribution of bare  $u$  and  $d$  quarks of the same mass  $M = 0.3$  GeV<sup>3</sup>. Only a significantly smaller constant mass  $\sim 0.2$  GeV close to the average one probed under the integrand leads to a result that compares with the dynamical one. Note, however, that this does not work in general, i.e. the fully dynamical result of  $47 \times 10^{-11}$  is not reproduced by a static approach with  $Z = 0.83$  and  $M = 0.14$  GeV.

### B. Impact of dressed vertices: Gauge Part

Here we focus upon the gauge part of the vertex. In the case of the ENJL model this part is just bare since  $Z_f = 1$ . In the DSE approach for the leading part, Eq. (22), we give the fully dynamical result in Table III. By comparison with the first value of Table II we find an increase by more than a factor of 2 when the vertex dressing is included. Again, this is roughly what one expects, since the contribution from the vertices gives a factor  $\sim \langle Z_f \rangle^{-4}$ . Note that the enhancement from the gauge-part of the vertex is comparable to the suppression due to a non-trivial  $Z_f$  in the quark propagator.

In principle, we should include not only the leading term of the gauge part of the vertex but the full Ball-Chiu vertex as fixed by the Ward-Takahashi identity. However, this is currently not possible due to numerical instabilities which are currently not under control<sup>4</sup>.

### C. Impact of dressed vertices: VMD Part

To better compare with the ENJL model we consider first the case where the quark-photon vertex is taken to be of the form

$$\Gamma_\mu(Q, k) = Z_2 \gamma_\mu + \tau^{(1)}(Q, k) T_\mu^{(1)}(Q, k), \quad (24)$$

with the leading transverse component  $T_\mu^{(1)}(Q, k) = \gamma_\mu^T$ , and  $\tau^{(1)}(Q, k)$  its dressing function. The quark wave function renormalisation constant  $Z_2$  is necessary to maintain multiplicative renormalizability. For the transverse dressing function  $\tau^{(1)}(Q, k)$  we study three choices: (i) the ENJL model, Eq. (17), which we also supplement by an additional factor

$$f(k^2) = 1/(1 + k^4/0.66^4) \quad (25)$$

to simulate a relative momentum dependence, (ii) the DSE approach with the numerical solution to Eq. (10) and (iii) the DSE approach with the analytic fit function Eq. (21) to the numerical result. Both, (ii) and (iii) already include a relative momentum dependence in contrast to the original ENJL approach. Our results are presented in Table IV.

First of all note that the result where a bare vertex  $Z_2 \gamma_\mu$  is used together with the ENJL type transverse part (first line) is quite close to the ENJL result shown in Eq. (23). We are thus able to reproduce the ENJL result numerically, despite the very different UV cutoff, that obviously does not matter much. Taking a closer look at Table IV we see a common pattern. When the vertices do not depend on the relative momentum between the two quarks, the contribution is around  $a_\mu \sim (14-16) \times 10^{-11}$ . Compared to the corresponding result with bare-vertex of  $47 \times 10^{-11}$  we therefore find a reduction of similar size as the one from  $\sim 60 \times 10^{-11}$  to  $\sim 20 \times 10^{-11}$  reported by [11]. We obtain this large suppression in our ENJL type calculation as well as in the DSE approach with momentum dependent quark propagators. However, when we take into account the relative momentum dependence in the full DSE calculation and including the additional factor  $f(k)$  in the ENJL model we find that the suppression due to transverse parts is much reduced. We find results in the range of  $a_\mu \sim (41-46) \times 10^{-11}$ . This is at most a reduction of just  $\sim 15\%$  and constitutes one of the main results of this work.

Finally, we give the same comparison with the inclusion of the leading  $L_1$  dressing  $\lambda^{(1)}$  from Eq. (22) given by the WTI, see Table V. We see that the trend here is very similar as for the bare vertex, except now with an enhancement due to the non-trivial dressing function of the gauge part. This enhancement is of the order of 2 – 3. It differs slightly for the cases with and without relative momentum dependence, which shows that there is also interference between the different vertex components. Note that the  $\lambda^{(1)}$  dressing is always used with its full kinematics.

### D. Best result and electromagnetic gauge invariance

Our most reliable estimate for the contribution from the quark-loop to the anomalous magnetic moment of the muon is the one obtained with full dynamics in the quark propagator, the leading gauge-part  $\lambda^{(1)}$  and the

<sup>3</sup> This number is extracted from Table I of Ref. [54]

<sup>4</sup> The corresponding results given in Ref. [20] are presumably not correct as will be detailed in an erratum.

Vertex Dressing	$a_\mu[10^{-11}]$
$Z_2\gamma_\mu + \gamma_\mu^T \tau_{\text{ENJL}}$	14
$Z_2\gamma_\mu + \gamma_\mu^T \tau_{\text{ENJL}} f(k^2)$	45
$Z_2\gamma_\mu + \gamma_\mu^T \tau_{\text{fit}}^{(1)}(k=0)$	16
$Z_2\gamma_\mu + \gamma_\mu^T \tau_{\text{fit}}^{(1)}$	46
$Z_2\gamma_\mu + \gamma_\mu^T \tau_{\text{calc}}^{(1)}(k=0)$	14
$Z_2\gamma_\mu + \gamma_\mu^T \tau_{\text{calc}}^{(1)}$	41

TABLE IV. Bare and leading transverse vertex component, with dressing functions from the ENJL model, VMD like fit from DSE/BSE ( $\tau_{\text{fit}}^{(1)}$ ), and from an explicit calculation of the quark-photon DSE ( $\tau_{\text{calc}}^{(1)}$ ). Results are shown with, and without the inclusion of a dependence on the relative momentum.

Vertex Dressing	$a_\mu[10^{-11}]$
$\gamma_\mu\lambda^{(1)} + \gamma_\mu^T \tau_{\text{ENJL}}$	43
$\gamma_\mu\lambda^{(1)} + \gamma_\mu^T \tau_{\text{ENJL}} f(k^2)$	103
$\gamma_\mu\lambda^{(1)} + \gamma_\mu^T \tau_{\text{fit}}^{(1)}(k=0)$	43
$\gamma_\mu\lambda^{(1)} + \gamma_\mu^T \tau_{\text{fit}}^{(1)}$	105
$\gamma_\mu\lambda^{(1)} + \gamma_\mu^T \tau_{\text{calc}}^{(1)}(k=0)$	41
$\gamma_\mu\lambda^{(1)} + \gamma_\mu^T \tau_{\text{calc}}^{(1)}$	96

TABLE V. 1BC and leading transverse vertex component, with dressing functions from the ENJL model, VMD like fit from DSE/BSE ( $\tau_{\text{fit}}^{(1)}$ ), and from an explicit calculation of the quark-photon DSE ( $\tau_{\text{calc}}^{(1)}$ ). Results are shown with, and without the inclusion of a dependence on the relative momentum.

leading transverse part  $\tau_{\text{calc}}^{(1)}$  of the quark-photon vertex. For two light quark flavors we obtained

$$a_\mu^{\text{LBL,L1+T1},N_f=2} = (96 \pm 2) \times 10^{-11}, \quad (26)$$

where the error is purely numerical. Compared to the corresponding value  $a_\mu^{\text{LBL,L1},N_f=2} = (100 \pm 2) \times 10^{-11}$  for the 1BC vertex without transverse parts we thus find a suppression of the order of five percent due to the VMD physics. This is much less than in simple models. If we additionally include the strange and charm quark contributions we arrive at

$$a_\mu^{\text{LBL,L1+T1},N_f=4} = (107 \pm 2) \times 10^{-11}, \quad (27)$$

which compares to the 1BC  $N_f = 4$  case (in Landau gauge)  $a_\mu^{\text{LBL,L1},N_f=4} = (111 \pm 2) \times 10^{-11}$ . Note once more that the corresponding result in [20] differs slightly due to QED Feynman-gauge, see discussion below.

We are currently working on the further inclusion of the other transverse terms  $\tau^{(2..8)}$ , corresponding results will be presented elsewhere. The potential impact of these terms is hard to gauge without an explicit calculation. Nevertheless, from a systematic point of view, the omission of these terms is unproblematic. This is different for the non-transverse part of the vertex. Strictly speaking, the presence of all three Ball-Chiu components

Interaction	$\xi$	$a_\mu^{\text{LBL,QL}} \times 10^{11}$
MT	0	96
MT	1	94

TABLE VI. Results for the 1BC+transverse vertex dressings. We compare different photon gauge parameters  $\xi = \{0, 1\}$ , i.e. Landau and Feynman gauge.

$\lambda^{(1..3)}$  are necessary to maintain electromagnetic gauge invariance. As mentioned above, this is currently not possible due to severe numerical problems with the terms  $\lambda^{(2)}$  and  $\lambda^{(3)}$ . We therefore have to gauge the error in the present calculation due to violations of gauge invariance. This is conveniently done by varying the QED gauge parameter  $\xi$ . Results for Feynman and Landau gauge are shown in table VI. The variations with  $\xi$  are on the two percent level and therefore reassuringly small. The insensitivity with respect to the gauge parameter is an indicator for the (almost) transversality of the resulting quark-loop part of the photon four-point function  $\Pi_{\mu\nu\alpha\beta}$ .

We emphasize, however, that the smallness of the gauge violations due to the omission of  $\lambda^{(2)}$  and  $\lambda^{(3)}$  cannot be taken as an indication that these terms will not contribute much to the physical, transverse part of the photon four-point functions. As already mentioned above, our previous calculation of these contributions in Ref. [20] is presumably not correct and needs to be thoroughly reinvestigated. This will be done in future work.

## VI. SUMMARY AND CONCLUSION

In this work we investigated in detail key similarities and differences between the ENJL and DSE approaches. Whereas the ENJL model features a contact interaction giving rise to a trivial quark wave-function renormalisation and a constant quark mass function, in the DSE approach these are both momentum dependent. The same is true for the gauge part of the vertex, that is determined by a Ward-Takahashi Identity. Whereas in the ENJL model this part is trivial, the corresponding Ball-Chiu terms in the DSE approach are nontrivial and momentum dependent. In both approaches there are transverse parts in the vertex which are dominated by the vector meson poles leading to a characteristic behavior also in the space-like momentum region.

When assessing the influence of the different momentum dependent dressing functions of the DSE approach as compared to ENJL we found partial cancellations. Dressing effects due to the non-trivial wave-function on the level of 50% are cancelled by opposite effects due to the dressing of the gauge part of the vertex. An important effect that is not cancelled is the one of the dynamical mass function. We found that this function is not tested predominantly at its large infrared plateau of  $M(0) \sim 0.48$  GeV but rather at smaller values at inter-

mediate momenta commensurate with  $M \sim 0.2$  GeV. This gives rise to a larger contribution than expected from constituent quark-loop calculations. Our finding may serve to explain the surprisingly small (constituent) quark masses needed in chiral models to obtain sensible results [17]. Our most interesting result, however, is related to the transverse part of the vertex. These are of high interest because they dynamically include the phenomenology of vector meson dominance and are expected to reduce the overall light-by-light contribution. As in the ENJL model the corresponding behavior of the transverse part of the vertex in the DSE-approach is generated dynamically. A key difference is, however, that in the DSE case the dependence on the relative momentum of the quarks is taken into account. On the level of mesons (as e.g. the  $\rho$ -meson that is the vital ingredient in VMD) this takes the distribution of quarks inside the bound state into account, which is not the case in the ENJL model [55]. The inclusion of this effect, either in the full DSE calculation or by a suitable modification of the VMD-term in the ENJL model has important consequences: the reduction of the quark-loop contribution to  $a_\mu$  due to VMD effects, observed in previous calculations [11], is drastically reduced.

Thus we can pinpoint the differences between the DSE and ENJL calculations to be down to the contact interaction limiting the momentum dependence of dressing functions. We believe that ignoring the relative quark momentum in the quark-photon vertex overestimates the suppression that the transverse part of the vertex provides and thus lowers significantly its numerical contribution to the anomalous magnetic moment of the muon.

Our present best result for the quark-loop contribution has been discussed in section VD. Combined with our result for the pseudoscalar meson exchange diagram from Ref. [20],  $a_\mu^{\text{LBL};PS} \approx (81 \pm 2) \times 10^{-11}$ , we arrive at the estimate

$$a_\mu^{\text{LBL}} = (188 \pm 4) \times 10^{-11}, \quad (28)$$

for the total LBL contribution. Again, the error is purely statistical due to our numerics. Since at present any guess of the systematic error of this number is clearly subjective (due to the omission of terms in the quark-photon vertex), we do not attempt such an estimate.

It has to be emphasized, however, that our determination of the quark loop contribution to light-by-light, Eq. (28) is by far not complete since several terms in the vertex dressing are still missing. The study if the influence of these terms is an important task for the future. Nevertheless we hope that the systematics of the present work serves to give the reader a better understanding of the technical and physical mechanisms at work in the complicated light-by-light scattering contribution. Furthermore we have shown that our best results at present are stable under variations of the photon gauge parameter and therefore serve as an important intermediary step

towards a full calculation to come.

### Acknowledgments

We are grateful to Fred Jegerlehner and Andreas Nyfeler for discussions. This work was supported by the Helmholtz International Center for FAIR within the LOEWE program of the State of Hesse, the Helmholtz Young Investigator Group under contract VH-NG-332 and DFG under contract FI 970/8-1, and the Austrian Science Fund FWF under project M1333-N16.

### Appendix A: Quark-photon vertex

In this appendix we give the explicit basis for the quark-photon vertex. It was taken from Ref. [32].

$$\begin{aligned} L_\mu^1 &= \gamma_\mu \\ L_\mu^2 &= 2k_\mu \not{k} \\ L_\mu^3 &= 2ik_\mu \\ L_\mu^4 &= i[\gamma_\mu, \gamma_\nu] k_\nu \\ T_\mu^1 &= \gamma_\mu^T \\ T_\mu^2 &= [k_\mu^T \not{k}^T - \frac{1}{3} \gamma_\mu^T (k^T)^2] / k^2 \\ T_\mu^3 &= k_\mu^T \not{P} \cdot k / (k^2 P^2) \\ T_\mu^4 &= -(\gamma_\mu^T [\not{P}, \not{k}^T] + 2k_\mu^T \not{P}) / 2k \\ T_\mu^5 &= ik_\mu^T / k \\ T_\mu^6 &= i[\gamma_\mu^T, \not{k}^T] P \cdot k / k^2 \\ T_\mu^7 &= i[\gamma_\mu^T, \not{P}] \left( 1 - \frac{(P \cdot k)^2}{P^2 k^2} \right) - 2T_\mu^8 \\ T_\mu^8 &= ik_\mu^T \not{k}^T \not{P} / k^2. \end{aligned} \quad (\text{A1})$$

Here  $P$  is the total momentum (photon momentum) and the relative momentum is  $k = (k_+ + k_-)/2$  were  $k_\pm$  are the quark momenta. The symbol  $T$  denotes transversality with respect to  $P$ . Furthermore,  $k = \sqrt{k^2}$ . The twelve dressing functions corresponding to the tensor structure (A1) are denoted as  $\lambda^{(i)}$ , ( $i = 1, 2, 3, 4$ ) corresponding to the  $L_\mu^{(i)}$  and  $\tau^{(j)}$  with ( $j = 1, \dots, 8$ ) corresponding to the  $T_\mu^{(j)}$ , see Eq. (20). The dressings  $\lambda^{(i)}$  are determined by the WTI

$$iP_\mu \Gamma_\mu(P, k) = S^{-1}(k_-) - S^{-1}(k_+). \quad (\text{A2})$$

and regularity demands [47]. The resulting vertex construction is referred to as the Ball-Chiu construction

$$\Gamma_\mu^{\text{BC}}(P, k) = \gamma_\mu \Sigma_A + 2\not{k} k_\mu \Delta_A + ik_\mu \Delta_B, \quad (\text{A3})$$

where the symbols

$$\Sigma_F = \frac{F(k_+^2) + F(k_-^2)}{2} \quad \Delta_F = \frac{F(k_+^2) - F(k_-^2)}{k_+^2 - k_-^2}, \quad (\text{A4})$$

have been used and  $A$  and  $B$  are the quark dressings. Note that  $\lambda^{(4)}$  is identically zero.

FIG. 6. The photon DSE. Full Propagators are denoted by white blobs and the red blob marks the full 1PI fermion-photon vertex.

### Appendix B: Derivation of the hadronic four-point function

In the present appendix we present the derivation of the photon four-point function that is needed in the light-by-light scattering contribution to the muon  $g - 2$ . The four-point function is obtained by taking two derivatives of the full inverse photon propagator

$$\begin{aligned} \Pi_{\mu\nu\alpha\beta} &= \frac{\delta^4 \Gamma[A]}{\delta A_\mu \delta A_\nu \delta A_\alpha \delta A_\beta} \\ &= \frac{\delta^2}{\delta A_\mu \delta A_\nu} \frac{\delta^2 \Gamma[A]}{\delta A_\alpha \delta A_\beta} = \frac{\delta^2}{\delta A_\mu \delta A_\nu} (D_{\alpha\beta})^{-1}. \end{aligned} \quad (\text{B1})$$

In order to proceed we consider the photon DSE that is presented in Fig. 6. We now take two further derivatives of the photon DSE. By the virtue of the approximation we consider, namely rainbow-ladder truncation of QCD, the photon is not a dynamical field in our formalism. The photon self-energy that we calculate is performed using quark and quark-photon vertex equations that do not take into account the photon as a dynamical object, but rather as an external background field. Internally all objects just include dynamical quarks and model gluons. This is why the application of further derivatives on the photon DSE is consistent within our approximation. Furthermore this operation leaves the internal consistency of the truncation intact. In particular the consistency with chiral symmetry and electro-magnetic current-conservation in form of WTI's is not destroyed. This technique is also referred to as 'gauging' [56]. For a detailed description of this procedure in particular in rainbow-ladder truncation see [57].

An object that will be needed on several occasions is the quark anti-quark photon-photon vertex. Within rainbow-ladder approximation this object can be exactly written in terms of quark-photon vertices and the T-matrix [57]

where the factor of two is not a symmetry factor but rather a convenient way to denote that the two possible photon permutations are included. Application of one

derivative to the photon DSE in Fig. 6 gives

The bare inverse photon does not contribute. The derivative has to be applied to the quark-photon vertex and the two dressed quarks of the photon self energy. Since there are two quarks in the loop the second diagram comes again with two permutations that correspond to one diagram with straight photon legs and one with crossed ones. This is signaled by the factor 2. Now the application of the relation shown in Eq. (B2) results in

Next we take into account the relation between the T-matrix and the G-matrix

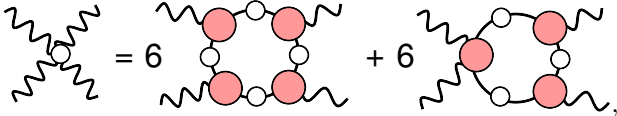
$$G = SS + SSTSS, \quad (\text{B3})$$

which says nothing but that the T-matrix is the amputated connected part of the G-matrix. In Eq. (B3),  $S$  is the quark propagator and multiplication indicates contraction of dirac-indices and integration over momentum arguments. The inhomogeneous part that involves just two propagators ( $SS$  in Eq. (B3)) cancels the second diagram on the right side of the equation above and we are left with

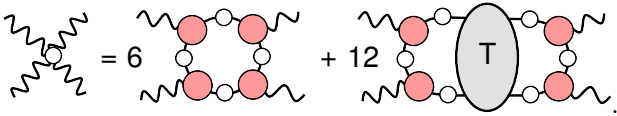
Now the final step is to remember that the bare quark-photon vertex together with the G-matrix corresponds to a dressed quark-photon vertex and to external quark-leg dressings. Finally we obtain the consistent representation of the hadronic part of the three-photon vertex

which is not zero as long as the external photon background-field is present. The factor 2 can also be interpreted as representing the two possible orientations of the quark loop.

Now the four-point function is obtained by taking a further derivative with respect to the external photon field. Again the derivative can act on quark-photon vertices and the quark propagators. The result is



where the additional factor three is caused by the three possible vertices and three propagators respectively. Using again relation (B2) we arrive at



Up to this point no approximations on top of rainbow-ladder truncation of QCD have been made. The last two representations of the four-point function are thus truly consistent with the rainbow-ladder photon self-energy shown in Fig. 6.

- 
- [1] **Muon G-2 Collaboration**, G. Bennett *et al.* *Phys.Rev.* **D73** (2006) 072003, [arXiv:hep-ex/0602035 \[hep-ex\]](#).
- [2] B. Roberts *Chin.Phys.* **C34** (2010) 741-744, [arXiv:1001.2898 \[hep-ex\]](#).
- [3] T. Aoyama, M. Hayakawa, T. Kinoshita, and M. Nio [arXiv:1205.5370 \[hep-ph\]](#).
- [4] A. Czarnecki, W. J. Marciano, and A. Vainshtein *Phys.Rev.* **D67** (2003) 073006, [arXiv:hep-ph/0212229 \[hep-ph\]](#).
- [5] F. Jegerlehner and A. Nyffeler *Phys.Rept.* **477** (2009) 1-110, [arXiv:0902.3360 \[hep-ph\]](#). 134 pages, 68 figures.
- [6] X. Feng, K. Jansen, M. Petschlies, and D. B. Renner *Phys.Rev.Lett.* **107** (2011) 081802, [arXiv:1103.4818 \[hep-lat\]](#).
- [7] P. Boyle, L. Del Debbio, E. Kerrane, and J. Zanotti [arXiv:1107.1497 \[hep-lat\]](#).
- [8] M. Della Morte, B. Jager, A. Juttner, and H. Wittig *JHEP* **1203** (2012) 055, [arXiv:1112.2894 \[hep-lat\]](#).
- [9] T. Goecke, C. S. Fischer, and R. Williams *Phys.Lett.* **B704** (2011) 211-217, [arXiv:1107.2588 \[hep-ph\]](#).
- [10] K. Hagiwara, R. Liao, A. D. Martin, D. Nomura, and T. Teubner *J.Phys.G* **G38** (2011) 085003, [arXiv:1105.3149 \[hep-ph\]](#).
- [11] J. Bijnens, E. Pallante, and J. Prades *Nucl.Phys.* **B474** (1996) 379-420, [arXiv:hep-ph/9511388 \[hep-ph\]](#).
- [12] M. Hayakawa, T. Kinoshita, and A. Sanda *Phys.Rev.Lett.* **75** (1995) 790-793, [arXiv:hep-ph/9503463 \[hep-ph\]](#).
- [13] M. Knecht and A. Nyffeler *Phys.Rev.* **D65** (2002) 073034, [arXiv:hep-ph/0111058 \[hep-ph\]](#).
- [14] K. Melnikov and A. Vainshtein *Phys.Rev.* **D70** (2004) 113006, [arXiv:hep-ph/0312226 \[hep-ph\]](#).
- [15] A. E. Dorokhov and W. Broniowski *Phys.Rev.* **D78** (2008) 073011, [arXiv:0805.0760 \[hep-ph\]](#).
- [16] A. Dorokhov, A. Radzhabov, and A. Zhevlakov [arXiv:1204.3729 \[hep-ph\]](#).
- [17] D. Greynat and E. de Rafael, *JHEP* **1207** (2012) 020 [arXiv:1204.3029 \[hep-ph\]](#).
- [18] L. Cappiello, O. Cata, and G. D'Ambrosio *Phys.Rev.* **D83** (2011) 093006, [arXiv:1009.1161 \[hep-ph\]](#).
- [19] C. S. Fischer, T. Goecke, and R. Williams *Eur.Phys.J.* **A47** (2011) 28, [arXiv:1009.5297 \[hep-ph\]](#).
- [20] T. Goecke, C. S. Fischer, and R. Williams *Phys.Rev.* **D83** (2011) 094006, [arXiv:1012.3886 \[hep-ph\]](#).
- [21] M. Hayakawa, T. Blum, T. Izubuchi, and N. Yamada *PoS LAT2005* (2006) 353, [arXiv:hep-lat/0509016 \[hep-lat\]](#); T. Blum, *Talk given at INT Workshop 11-47W (2011)*; K. Jansen, *Talk given at MesonNet Workshop on Meson Transition Form Factors (2012)*.
- [22] J. Prades, E. de Rafael, and A. Vainshtein [arXiv:0901.0306 \[hep-ph\]](#).
- [23] G. Venanzoni, *J. Phys. Conf. Ser.* **349** (2012) 012008, [arXiv:1203.1501 \[hep-ex\]](#). E989 experiment at Fermilab: <http://gm2.fnal.gov/>.
- [24] J. Aldins, T. Kinoshita, S. J. Brodsky, and A. Dufner *Phys.Rev.* **D1** (1970) 2378.
- [25] C. S. Fischer and R. Williams *Phys.Rev.* **D78** (2008) 074006, [arXiv:0808.3372 \[hep-ph\]](#).
- [26] C. S. Fischer and R. Williams *Phys.Rev.Lett.* **103** (2009) 122001, [arXiv:0905.2291 \[hep-ph\]](#).
- [27] R. Alkofer, C. S. Fischer, and R. Williams *Eur.Phys.J.* **A38** (2008) 53-60, [arXiv:0804.3478 \[hep-ph\]](#).
- [28] L. Chang and C. D. Roberts, *Phys. Rev. Lett.* **103** (2009) 081601, [arXiv:0903.5461 \[nucl-th\]](#).
- [29] A. Bashir, L. Chang, I. C. Cloet, B. El-Bennich, Y.-x. Liu, *et al. Commun. Theor. Phys.* **58** (2012) 79 [arXiv:1201.3366 \[nucl-th\]](#).
- [30] P. Maris and C. D. Roberts *Phys.Rev.* **C56** (1997) 3369-3383, [arXiv:nucl-th/9708029 \[nucl-th\]](#).
- [31] P. Maris and P. C. Tandy *Phys.Rev.* **C60** (1999) 055214, [arXiv:nucl-th/9905056 \[nucl-th\]](#).
- [32] P. Maris and P. C. Tandy *Phys.Rev.* **C61** (2000) 045202, [arXiv:nucl-th/9910033 \[nucl-th\]](#).
- [33] D. Jarecke, P. Maris, and P. C. Tandy *Phys.Rev.* **C67** (2003) 035202, [arXiv:nucl-th/0208019 \[nucl-th\]](#).
- [34] P. Maris and P. C. Tandy *Phys.Rev.* **C65** (2002) 045211, [arXiv:nucl-th/0201017 \[nucl-th\]](#).
- [35] G. Eichmann, R. Alkofer, A. Krassnigg, and D. Nicmorus *Phys.Rev.Lett.* **104** (2010) 201601, [arXiv:0912.2246 \[hep-ph\]](#).
- [36] G. Eichmann *Phys.Rev.* **D84** (2011) 014014, [arXiv:1104.4505 \[hep-ph\]](#).
- [37] G. Eichmann and C. S. Fischer, *Eur. Phys. J. A* **48** (2012) 9, [arXiv:1111.2614 \[hep-ph\]](#).
- [38] H. Sanchis-Alepuz, G. Eichmann, S. Villalba-Chavez, and R. Alkofer *Phys.Rev.* **D84** (2011) 096003, [arXiv:1109.0199 \[hep-ph\]](#); H. Sanchis-Alepuz, R. Alkofer, G. Eichmann, and R. Williams *PoS QCD-TNT-II* (2011) 041, [arXiv:1112.3214 \[hep-ph\]](#);

- H. Sanchis-Alepuz, R. Alkofer, and R. Williams *PoS QNP2012* (2012) 112, [arXiv:1206.6599 \[hep-ph\]](#).
- [39] P. Maris, C. D. Roberts, and P. C. Tandy *Phys. Lett. B* **420** (1998) 267–273, [arXiv:nucl-th/9707003](#).
- [40] H. Munczek *Phys.Rev.* **D52** (1995) 4736–4740, [arXiv:hep-th/9411239 \[hep-th\]](#).
- [41] J. Bijnens, E. Pallante, and J. Prades *Nucl.Phys.* **B626** (2002) 410–411, [arXiv:hep-ph/0112255 \[hep-ph\]](#).
- [42] M. Hayakawa, T. Kinoshita, and A. Sanda *Phys.Rev.* **D54** (1996) 3137–3153, [arXiv:hep-ph/9601310 \[hep-ph\]](#).
- [43] M. Hayakawa and T. Kinoshita *Phys.Rev.* **D57** (1998) 465–477, [arXiv:hep-ph/9708227 \[hep-ph\]](#).
- [44] M. Hayakawa and T. Kinoshita [arXiv:hep-ph/0112102 \[hep-ph\]](#).
- [45] A. Nyffeler *PoS CD09* (2009) 080, [arXiv:0912.1441 \[hep-ph\]](#).
- [46] A. Dorokhov, A. Radzhabov, and A. Zhevlakov *Eur.Phys.J.* **C71** (2011) 1702, [arXiv:1103.2042 \[hep-ph\]](#).
- [47] J. S. Ball and T.-W. Chiu *Phys.Rev.* **D22** (1980) 2542.
- [48] C. S. Fischer, D. Nickel, and J. Wambach *Phys.Rev.* **D76** (2007) 094009, [arXiv:0705.4407 \[hep-ph\]](#).
- [49] K. T. Engel, H. H. Patel and M. J. Ramsey-Musolf, *Phys.Rev.* **D86** (2012) 037502, [arXiv:1201.0809 \[hep-ph\]](#)
- [50] J. Bijnens *Phys.Rept.* **265** (1996) 369–446, [arXiv:hep-ph/9502335 \[hep-ph\]](#).
- [51] J. Bijnens and J. Prades *Z.Phys.* **C64** (1994) 475–494, [arXiv:hep-ph/9403233 \[hep-ph\]](#).
- [52] R. Boughezal and K. Melnikov *Phys.Lett.* **B704** (2011) 193–196, [arXiv:1104.4510 \[hep-ph\]](#).
- [53] T. Hahn *Comput.Phys.Commun.* **168** (2005) 78–95, [arXiv:hep-ph/0404043 \[hep-ph\]](#).
- [54] T. Kinoshita, B. Nizic and Y. Okamoto, *Phys. Rev. D* **31** (1985) 2108.
- [55] P. C. Tandy *Prog.Part.Nucl.Phys.* **39** (1997) 117–199, [arXiv:nucl-th/9705018 \[nucl-th\]](#).
- [56] H. Haberzettl, *Phys. Rev. C* **56**, 2041 (1997), [arXiv:nucl-th/9704057](#).
- [57] G. Eichmann, C. S. Fischer, *Phys.Rev.* **D85** (2012) 034015, [arXiv:1111.0197 \[hep-ph\]](#)